Unconventional filling factor of 4/11: A closed-form ground-state wave function

Sahana Das [1], Sudipto Das [2], and Sudhansu S. Mandal [1,2]
[1]*Centre for Theoretical Studies, Indian Institute of Technology, Kharagpur 721302, West Bengal, India*
[2]*Department of Physics, Indian Institute of Technology, Kharagpur 721302, West Bengal, India*

(Received 13 November 2020; revised 27 January 2021; accepted 27 January 2021; published 11 February 2021)

The ground state at 4/11 filling factor is very well understood, Mukherjee *et al.* [Phys. Rev. Lett. **112**, 016801 (2014)] in terms of the 1/3-filled second effective Landau level of the composite fermions whose correlations resemble that of electrons in the ground state of a two-body Haldane pseudo-potential of relative angular momentum 3, V_3. We here propose a closed-form ground-state wave function for V_3 at 1/3 filling factor. We successfully compare it with the exact wave function for systems with a few electrons by calculating their mutual overlap, pair-correlation function, and entanglement spectra. By numerical exact diagonalization for a few electron systems, we find a window of nonzero V_3 is essential together with V_1 for being 4/11 state incompressible. The constructed wave function for the 4/11 state using this proposed wave function has satisfactorily high overlap with previously studied composite-fermion-diagonalized ground-state wave function.

DOI: 10.1103/PhysRevB.103.075304

I. INTRODUCTION

Most of the fractional quantum Hall effect (FQHE) [1,2] in the lowest Landau level (LL) belonging to the sequences of filling factors $\nu = n/(2pn \pm 1)$ and $1 - n/(2pn \pm 1)$ are generally understood as a $\nu^* = n$ integer quantum Hall effect [3] (integer number of the filled effective LL, called Λ level) of composite fermions (CFs) [4,5] carrying $2p$ vortices, denoted as ^{2p}CFs. Amongst many other unconventional FQHE states in the lowest and higher LLs, the FQHE states in the range $1/3 < \nu < 2/5$ are particularly intriguing [6]. The states such as 4/11, 5/13, 3/8, and 6/17 within this range are observed in the experiments [7–9], although the latter two are not yet fully confirmed as there are no hints of flattening of the corresponding Hall resistances. These states correspond to respective fractional fillings $\nu^* = 1 + 1/3$, $1 + 2/3$, $1 + 1/2$, and $1 + 1/5$ of ^{2}CFs, i.e., $\Lambda = 0$ is completely filled and $\Lambda = 1$ is partially filled with respective fractions $\bar{\nu} = 1/3$, 2/3, 1/2, and 1/5. The neutral modes of excitations of these states display extremely low magnetoroton energies [10]. While $\bar{\nu} = 1/5$ seems to be a conventional [11] FQHE of CFs, the correlations for other three states can only be understood through unconventional [12–14] mechanisms: (i) Moore-Read Pfaffian [15] correlation, which is the exact ground state for a short-ranged three-body potential at $\bar{\nu} = 1/2$; (ii) Wojs-Yi-Quinn (WYQ) correlation [16], i.e., the ground state of a two-body Haldane pseudopotential [17] V_3 (where V_m is the model potential with two-body relative angular momentum m), at $\bar{\nu} = 1/3$ and its particle-hole conjugate partner 2/3. However, the absence of a suitable trial wave function of $\bar{\nu} = 1/3$ in the literature eludes us for knowing a closed-form ground-state wave function for $\nu = 4/11$ and further investigations of its properties.

Our primary focus in this paper is proposing a trial wave function of 1/3 WYQ state through several validity checks such as overlap with the exact wave function for a few electron systems, pair-correlation function [18] and qualitative low-energy features of the corresponding neutral mode in the single-mode approximation [19], and entanglement spectra (ES) [20]. Unlike the Laughlin state [2], the counting of states in the ES is found to be consistent with two Abelian edge modes [21]. The satisfactorily well trial wave function for WYQ state enables us to construct a closed-form ground-state wave function at $\nu = 4/11$ that has high overlap with the previously found composite-fermion diagonalized (CFD) ground state [13]. In addition, we investigate why the wave function for a V_3 model potential is necessary for understanding the 4/11 state while its neighboring conventional states 1/3 and 2/5 are well understood [5] only through the model potential V_1.

A two-body interaction operator $\hat{V}$ for fermions confined in the lowest LL, in general, may be expressed in terms of two-particle projection operators $|m\rangle\langle m|$ as $\hat{V} = \sum_{m\,(\text{odd})} V_m |m\rangle\langle m|$, where $|m\rangle$ denotes the two-particle state with relative angular momentum m, and V_m is the so-called Haldane pseudopotential [17] describing energy of the state $|m\rangle$. For the Coulomb interaction in the lowest LL, V_1 dominates over other pseudopotentials. The Laughlin wave function at $\nu = 1/3$ with flux-shift 3, i.e., number of flux quanta, $N_\phi = 3N - 3$, is the exact ground state of V_1 and the other conventional FQHE states with filling factors $\nu = n/(2n \pm 1)$ can be reproduced by the model potential V_1 only. The Laughlin wave function for $\nu = 1/5$ with $N_\phi = 5N - 5$ is the zero-energy ground state for $V_1 = V_3 \neq 0$ and vanishing other higher order pseudopotential components. The WYQ state [16] at $\nu = 1/3$ corresponding to the ground state of V_3 occurs for $N_\phi = 3N - 7$. The pseudopotential V_3 for CFs dominates over V_1 for the effective interaction between ^{2}CFs in the second Λ level [22,23]. Therefore, the FQHE of ^{2}CFs in $\Lambda = 1$ should primarily be feasible for V_3 only. This is why the ground-state wave function for $\nu = 4/11$ that corresponds

to 1/3 FQHE of ^{2}CFs in $\Lambda = 1$ are well-described [13] by the WYQ correlation.

In Sec. II, we begin by ruling out a simple possibility of a trial wave function like an extension to the CF wave function when only the third effective LL is completely filled, as the trial wave function for the WYQ state at $\nu = 1/3$. We then propose a successful trial wave function for this state as we find its reasonably high overlap with the exact ground state up to 14 electrons. We have also shown that overlap with the exact wave function may further be substantially improved by incorporating a simple extension of this proposed wave function by their suitable superpositions. For further checking the consistency of the proposed wave function, we calculate pair-correlation function, neutral mode of excitation within the single-mode approximation, and ES that are qualitatively and even quantitatively close to that for the exact state. Although the minimum gap for the neutral mode is an order of magnitude lower than the Laughlin state at the same filling factor, the finite gap ensures that the wave function represents an incompressible state. The low-lying ES indicates the label counting of the edge states as $1, 2, 5, \ldots$, suggesting two Abelian edge modes [21] for the WYQ 1/3 state. The trial wave function for WYQ 1/3 state is then used to construct a trial wave function for the 4/11 state in Sec. III. This wave function has been shown to have high overlap with the CFD [24] ground state [13], which is close to the exact state. In Sec. IV, we obtain a phase diagram in V_1–V_3 parameter space and identify the region for which 4/11 becomes an incompressible state. The phase diagram indicates that a window of V_3 needs to be essentially mixed with V_1 for an incompressible 4/11 state, consistent with our constructed wave function which consists of a part that is incompressible for the V_3 pseudopotential. Section V is devoted to a discussion about the future direction of study. In Appendix A, we have developed a method for how a many-body wave function in spherical geometry can be decomposed into the linear combination of determinants of occupied single-particle basis states. In Appendix B, we have reexpressed single-particle basis functions [5] of the lowest two Λ levels in a form [25] which shows similarity with the basis functions in a disk geometry [5]. Appendix C shows how a many-body wave function for the lowest LL can be recast for the $\Lambda = 1$ level.

II. TRIAL WAVE FUNCTION FOR WYQ 1/3 STATE

Since the WYQ 1/3 state occurs for $N_\phi = 3N - 7$ in contrast to $N_\phi = 3N - 3$ for the Laughlin wave function,

$$\Psi_L^{1/3} = \prod_{i<j}(u_i v_j - u_j v_i)^3, \tag{1}$$

which is also same as the CF wave function [4,5], it is tempting to write a trial wave function

$$\Psi_{\mathrm{CF},2}^{1/3} = \mathrm{P}_{\mathrm{LLL}} \prod_{i<j}(u_i v_j - u_j v_i)^2 \, \chi_2(\{u_i,\ v_i\}), \tag{2}$$

where χ_2 is the wave function for the $\Lambda = 2$ level being completely filled by the CFs while keeping the lower Λ levels with $\Lambda = 0$ and 1 completely empty, and $\mathrm{P}_{\mathrm{LLL}}$ represents projection onto the lowest LL. Here $u_j = \cos(\theta_j/2)e^{i\phi_j/2}$ and $v_j = \sin(\theta_j/2)e^{-i\phi_j/2}$ are the spherical spinors in terms of spherical coordinates for jth electron in a spherical geometry [17] of radius $R = \sqrt{Q}$ in the unit of magnetic length, $\ell = (\hbar c/eB)^{1/2}$, with magnetic monopole charge $Q = N_\phi/2$ residing at the center of the sphere. Since the overlap of $\Psi_{\mathrm{CF},2}$ with the exact ground state has not been found to be impressive (Table I), it cannot be considered as a satisfactory trial wave function.

TABLE I. Overlaps of the wave function $\Psi_{V_3}^{1/3}$ with $\Psi_{\mathrm{CF},2}^{1/3}$, $\Psi_{\mathrm{L-R}}^{1/3}$, and $\Psi_{\mathrm{L-MR}}^{1/3}$ including appropriate normalizations at $\nu = 1/3$ for N electrons. The numbers in (..) indicate the Monte Carlo uncertainty in the last significant digits. *For $N = 5$, $\Psi_{\mathrm{CF},2}^{1/3}$ identically vanishes. $\Psi_{\mathrm{L-R}}^{1/3}$ is exact for $N = 5$.

N	$\langle\Psi_{V_3}^{1/3}\vert\Psi_{\mathrm{CF},2}^{1/3}\rangle$	$\langle\Psi_{V_3}^{1/3}\vert\Psi_{\mathrm{L-R}}^{1/3}\rangle$	$\langle\Psi_{V_3}^{1/3}\vert\Psi_{\mathrm{L-MR}}^{1/3}\rangle$
5*	–	1.0	–
6	0.299(2)	0.89017	0.99762
7	0.213(2)	0.91661	0.95505
8	0.205(3)	0.88519	0.92107
9	0.158(5)	0.76491	0.90428
10	–	0.72486	0.86071
11	–	0.753(4)	0.863(2)
12	–	0.773(6)	0.854(2)
13	–	0.781(3)	0.836(2)
14	–	0.777(2)	0.824(1)

We here propose the ground-state wave function of V_3 at 1/3 as

$$\Psi_{\mathrm{L-R}}^{1/3}(\{u_i,\ v_i\}) = \prod_{i<j}^{N}(u_i v_j - v_i u_j)^3 \, \mathcal{S}\,(\mathcal{R}_N)\,, \tag{3}$$

$$\mathcal{R}_N = \left[\prod_{i=1}^{N}(u_i v_{i+1} - v_i u_{i+1})^{-2}\right], \tag{4}$$

where the extra factor $\mathcal{R}_N$ represents a ring correlation between N electrons; electrons are arranged in a closed ring (see Fig. 1) with $u_{N+1} = u_1$ and $v_{N+1} = v_1$. Here $\mathcal{S}$ represents the symmetrization for N identical particles. It is easy to check that the angular momentum of the wave function Eq. (3), $L = 0$. Although there appears a singularity in $\mathcal{R}_N$ when two electrons are closed, it is removed in $\Psi_{L-R}^{1/3}$ and Pauli exclusion principle is restored. The corresponding wave function in the disk geometry will read (by dropping ubiquitous Gaussian factor)

$$\Psi_{\mathrm{L-R}}^{1/3}(\{z_j\}) = \prod_{i<j}^{N}(z_i - z_j)^3 \, \mathcal{S}\left(\prod_{i=1}^{N}(z_i - z_{i+1})^{-2}\right), \tag{5}$$

with $z_j = (x_j - iy_j)/\ell$ and $z_{N+1} = z_1$.

We determine the ground-state wave function $\Psi_{V_3}^{1/3}$ by exactly diagonalizing [26] the pseudopotential V_3 with $N_\phi = 3N - 7$. The incompressible (the lowest energy state is at $L = 0$ only) ground state is obtained for $N \geqslant 5$. The overlap between $\Psi_{V_3}^{1/3}$ and $\Psi_{\mathrm{L-R}}^{1/3}$, $\langle\Psi_{V_3}^{1/3}\vert\Psi_{\mathrm{L-R}}^{1/3}\rangle$ obtained by the method of decomposition into the single-particle eigenbasis (DSPEB) introduced here (see Appendix A) for smaller N

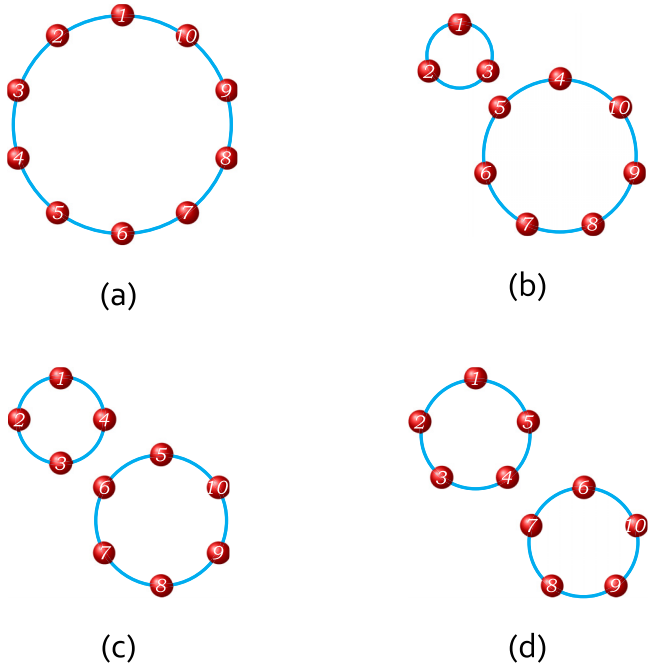

FIG. 1. Schematic arrangement of ten particles in closed rings where spheres represent electrons and the connecting lines between ith and jth electrons represent the function $(u_i v_j - v_i u_j)^{-2}$. Diagrammatic representations of the ring functions: (a) $\mathcal{R}_{10}$, (b) $\mathcal{R}_7\mathcal{R}_3$, (c) $\mathcal{R}_6\mathcal{R}_4$, and (d) $\mathcal{R}_5\mathcal{R}_5$.

and by the Monte Carlo method in the Metropolis algorithm for larger N is tabulated in Table I. While the latter method has statistical uncertainty, the former provides an exact value, albeit limited to a lesser number of particles. We find that $\Psi^{1/3}_{L-R}$ is exact for $N = 5$, but the overlap somewhat decreases with the increase of N. However, much improved overlap is obtained by mixing functions $\mathcal{R}_N$ with $\mathcal{R}_{N-k}\mathcal{R}_k$ where $k = 3, 4, \ldots, (N-1)/2$ $(N/2)$ for odd (even) N. Here $k_{\min} = 3$ because a ring is possible for at least three particles. These rings for $N = 10$ are schematically shown in Fig. 1 and the corresponding variational ground-state wave function is denoted as $\Psi^{1/3}_{\mathrm{L-MR}}$. The weight factors of the wave functions (not mutually orthogonal) constructed with ring functions $\mathcal{R}_{N-k}\mathcal{R}_k$ in $\Psi^{1/3}_{\mathrm{L-MR}}$ are tabulated in Table II. As the construction of exact real space wave function in each Monte Carlo step becomes computationally expensive for larger N due to exponential growth of basis states, we are able to compare our proposed wave function with the exact wave function up to $N = 14$ only for which the number of basis states is $\sim 4.8 \times 10^7$. The overlap $\langle \Psi^{1/3}_{V_3} | \Psi^{1/3}_{\mathrm{L-MR}} \rangle$ decreases with N, yet it seems to have a reasonably high value in the thermodynamic limit (Fig. 2). Although the overlap $\langle \Psi^{1/3}_{V_3} | \Psi^{1/3}_{\mathrm{L-R}} \rangle$ decreases very fast with the increase in N up to $N = 10$, thereafter it slowly increases with N and approaches $\langle \Psi^{1/3}_{V_3} | \Psi^{1/3}_{\mathrm{L-MR}} \rangle$.

Having shown $\Psi^{1/3}_{\mathrm{L-MR}}$ is a variationally improved trial wave function above, we find below that $\Psi^{1/3}_{\mathrm{L-R}}$ is indeed a topologically sufficient trial wave function for the WYQ 1/3 state by comparing the corresponding pair-correlation function, neutral mode of excitation, and the state counting in the low-lying sector of the ES with that of the exact ground state. $\Psi^{1/3}_{\mathrm{L-R}}$ is thus adiabatically connected to $\Psi^{1/3}_{\mathrm{L-MR}}$ and $\Psi^{1/3}_{V_3}$, and in turn topologically distinct from $\Psi^{1/3}_{\mathrm{L}}$.

TABLE II. Weight factors with signs of different normalized ring wave functions (up to two rings) in $\Psi^{1/3}_{\mathrm{L-MR}}$. We note that the sum of the square of the weight factors are not necessarily one as the ring wave functions are not mutually orthogonal.

N	$\mathcal{R}_N$	$\mathcal{R}_{N-3}\mathcal{R}_3$	$\mathcal{R}_{N-4}\mathcal{R}_4$	$\mathcal{R}_{N-5}\mathcal{R}_5$	$\mathcal{R}_{N-6}\mathcal{R}_6$	$\mathcal{R}_{N-7}\mathcal{R}_7$
5	1.0	–	–	–	–	–
6	0.779	−0.465	–	–	–	–
7	0.817	−0.315	–	–	–	–
8	0.764	−0.315	−0.126	–	–	–
9	0.423	−0.612	−0.196	–	–	–
10	0.374	−0.579	−0.278	−0.096	–	–
11	0.348	−0.473	−0.372	−0.160	–	–
12	0.380	−0.344	−0.382	−0.212	−0.126	–
13	0.426	−0.231	−0.313	−0.242	−0.175	–
14	0.414	−0.172	−0.250	−0.268	−0.218	−0.147

A. Pair-correlation and neutral mode

In Fig. 3, we show pair correlation function $g(r) = \frac{1}{N\rho_0}\langle \sum_{i<j} \delta(\boldsymbol{r} - \boldsymbol{r}_{ij}) \rangle$ with mean electron density ρ_0 and interparticle separation $\boldsymbol{r}_{ij} = \boldsymbol{r}_i - \boldsymbol{r}_j$ for $N = 10$ in the ground states of $\Psi^{1/3}_{V_3}$ and $\Psi^{1/3}_{\mathrm{L-R}}$. The simple trial wave function $\Psi^{1/3}_{\mathrm{L-R}}$ satisfactorily reproduces all the essential features of $g(r)$ that one finds with the exact state, in particular, the unusual (not present for Laughlin state [18]) hump appears (usually found for non-Abelian states like the Moore-Read state [29]) at $r \sim 2.5\ell$. These $g(r)$ are then exploited to determine neutral modes of excitations by the method of single mode approximation which was originally developed by Girvin-MacDonald-Platzman (GMP) [19,28]. The mode is determined by using a previously derived expression

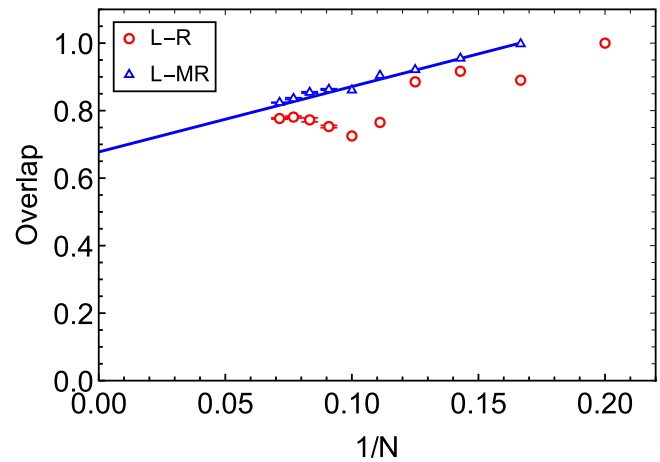

FIG. 2. Overlaps $\langle \Psi^{1/3}_{V_3} | \Psi^{1/3}_{\mathrm{L-R}} \rangle$ and $\langle \Psi^{1/3}_{V_3} | \Psi^{1/3}_{\mathrm{L-MR}} \rangle$ tabulated in Table I versus $1/N$. The line is a guide to the eye.

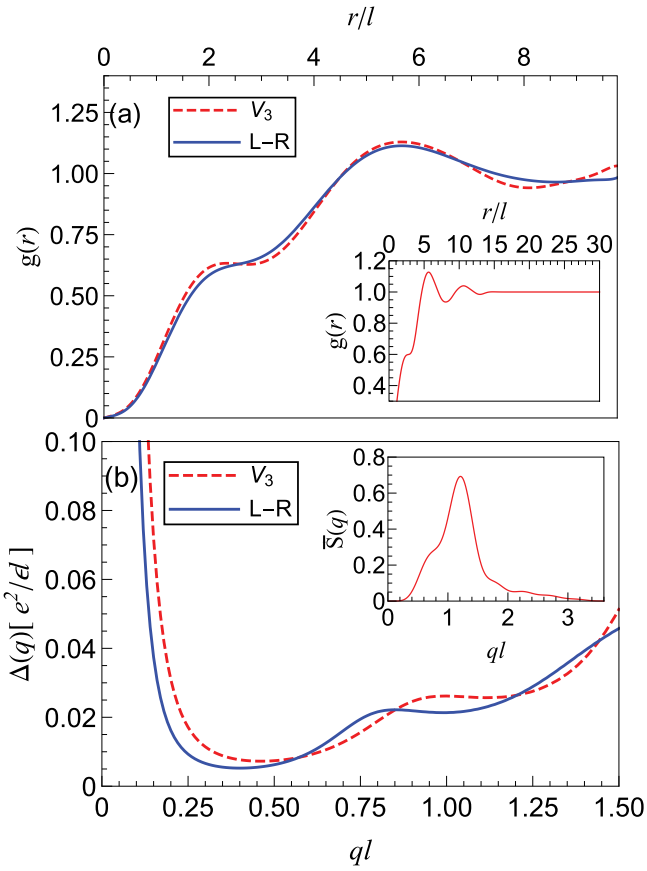

FIG. 3. Top panel: (a) Pair correlation function obtained for $N = 10$ using the wave functions $\Psi^{1/3}_{V_3}$ (dashed line) and $\Psi^{1/3}_{L-R}$ (solid line); Inset: Thermodynamic extrapolation of $g(r)$ for the wave function $\Psi^{1/3}_{V_3}$ in the damped-oscillatory form [27] $g(r) = 1 + A(r/\ell)^{-\alpha}\sin(\beta r/\ell - \gamma)$ used earlier for the oscillatory part, where A, α, β, and γ are numerical constants. Bottom panel: (b) Dispersion of the GMP mode $\Delta(q)$. Inset: The lowest LL-projected structure factor $\bar{S}(q)$ calculated using thermodynamically extrapolated $g(r)$ and further fitting with the GMP form [19,28] $g(r) = 1 - e^{-r^2/(2\ell^2)} + \sum_{m\,(\mathrm{odd})}(2/m!)(r^2/4\ell^2)^m c_m e^{-r^2/(4\ell^2)}$, where the coefficients c_m [up to a suitable maximum value of m for picking up the oscillations in $g(r)$] are to be determined by fitting.

[19,28]

$$\Delta(q) = 2(\bar{S}(q))^{-1}\int \frac{d\mathbf{k}}{(2\pi)^2}\sin^2\left(\frac{\mathbf{q}\times\mathbf{k}}{2}\ell^2\right)e^{-q^2\ell^2/2} \times\left[v(|\mathbf{k}-\mathbf{q}|)e^{\mathbf{q}\cdot(\mathbf{k}-\mathbf{q}/2)\ell^2} - v(k)\right]\bar{S}(k), \quad (6)$$

where projected structure factor $\bar{S}(k) = S(k) - 1 + e^{-k^2\ell^2/2}$ and $v(q) = (\frac{2\pi e^2}{\epsilon q})e^{-q^2\ell^2}L_3(q^2\ell^2)$ is the momentum-dependent potential [30] corresponding to the V_3 pseudopotential component of the Coulomb interaction. Here $S(k) = 1 + n_0\int d\boldsymbol{r}e^{i\boldsymbol{k}\cdot\boldsymbol{r}}[g(r) - 1]$ is the static structure factor, where the mean electron density $n_0 = \nu/2\pi\ell^2$ and $L_3(q^2\ell^2)$ is the third-order Laguerre polynomial. The neutral modes for $\Psi^{1/3}_{\mathrm{L-R}}$ agrees quite well with that for $\Psi^{1/3}_{V_3}$. Unlike [28] the Laughlin wave function, both of these show two side-by-side roton minima and the minimum gap is much lower than the Laughlin state.

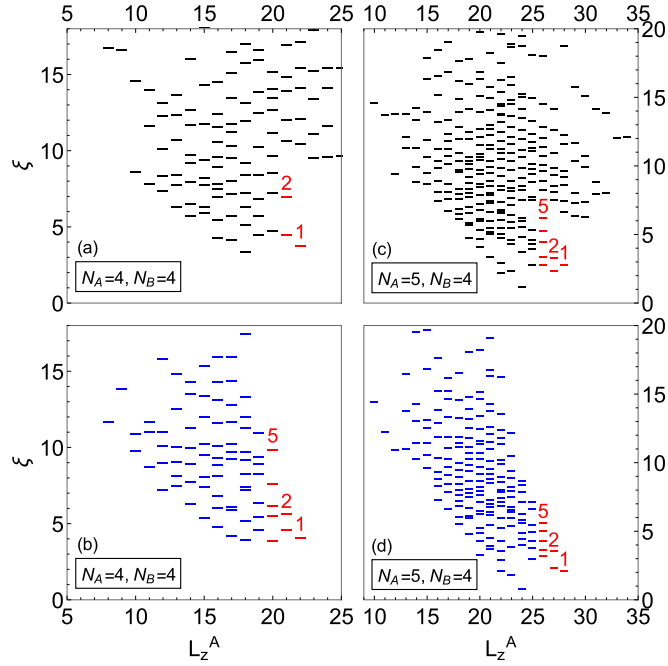

FIG. 4. Entanglement spectra obtained by the method of particle partitioning in real space. N_A (N_B) is the number of particles in northern (southern) hemisphere of the spherical geometry. L_z^A is the z component of the total orbital angular momentum of subsystem A. (a) and (b), respectively, for $\Psi^{1/3}_{V_3}$ and $\Psi^{1/3}_{\mathrm{L-R}}$ with $N_A = 4$ and $N_B = 4$. (c), (d), respectively, for $\Psi^{1/3}_{V_3}$ and $\Psi^{1/3}_{\mathrm{L-R}}$ with $N_A = 5$ and $N_B = 4$. The counting of low-lying levels (starting from the maximum value of $L_z^A = 22$ for the system $N = 8$ electrons and $L_z^A = 28$ for $N = 9$) for $\Psi^{1/3}_{\mathrm{L-R}}$ is in agreement with that for $\Psi^{1/3}_{V_3}$. The low-lying levels are counted as 1, 2, 5,....

B. Entanglement spectra

The state counting in the low-lying ES [20,31–35] has now been routinely used for determining the number of states at the edges [21] of FQHE systems. It therefore has been very useful for determining the topological nature of a FQHE state. The entanglement spectrum of an incompressible ground state is characterized by an entanglement gap separating low-lying spectrum from the high-energy sector [36].

The ES are generally obtained by partitioning the system into two subsystems in a number of ways, namely, orbital partitions, particle partitions, and partitions in real space. Here, we employ the method described in Ref. [33] by dividing the sphere into two hemispheres A (upper hemisphere) and B (lower hemisphere), so the Fock space of the Hamiltonian $\mathcal{H}$ is partitioned into two parts $\mathcal{H}_A \otimes \mathcal{H}_B$. Using Schmidt decomposition [37], a many-body ground-state wave function for the whole system can be decomposed into the linear combination of the products of states in two subsystems,

$$|\psi\rangle = \sum_i e^{-(1/2)\xi_i}\left|\psi^i_A\right\rangle \otimes \left|\psi^i_B\right\rangle, \quad (7)$$

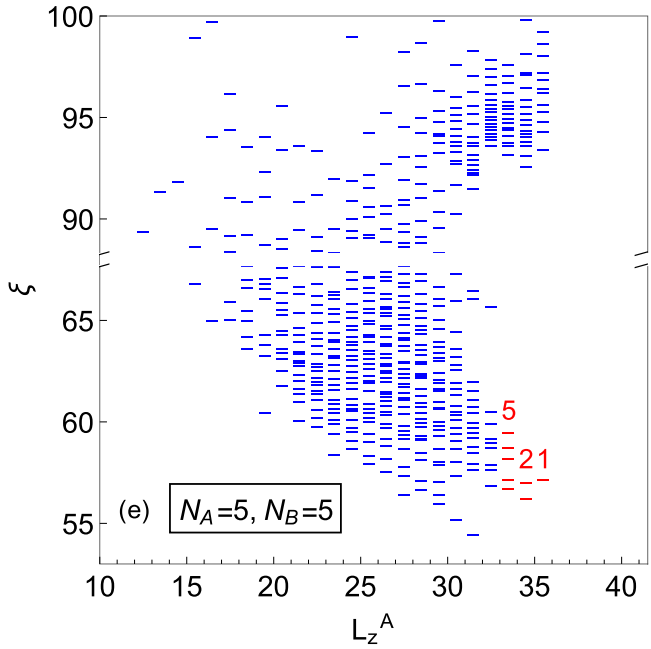

FIG. 5. Entanglement spectra with particle partitioning for $\Psi^{1/3}_{\mathrm{L-R}}$ as described in the caption of Fig. 4. Here $N_A = N_B = 5\,(N = 10)$ and the low-lying spectra starts from maximum value of $L_z^A = 35.5$. The low-lying level counting is found as 1, 2, 5, …, which matches with the counting of *two* chiral edge modes [21].

where, $|\psi_A^i\rangle \in \mathcal{H}_A$, $|\psi_B^i\rangle \in \mathcal{H}_B$, $\langle\psi_A^i|\psi_A^i\rangle = \langle\psi_B^i|\psi_B^i\rangle = \delta_{ij}$ and ξ_i represents entanglement energy for the ith state. Therefore, ξ_i can be obtained by diagonalizing the reduced density matrix for a subsystem, say A, i.e., $\hat{\rho}_A$ which may be obtained by tracing over B degrees of freedom of the full density matrix: $\hat{\rho}_A = \mathrm{Tr}_B[\hat{\rho}]$. If the subsystems contain N_A and N_B numbers of electrons, respectively, the total azimuthal angular momentum of the subsystems, $L_z^{A/B} = \sum_{k=1}^{N_A/N_B} l_z^k$ with $l_z^k = -Q, \ldots, +Q$ [l_z^k is positive (negative) in $A\,(B)$]. We determine ES for each L_z^A separately. In Fig. 4, we compare ES for $N = 8$ and 9 electrons calculated using the trial wave function $\Psi^{1/3}_{\mathrm{L-R}}$ with that for the exact wave function $\Psi^{1/3}_{V_3}$ of WYQ state at 1/3 filling. The state counting for the low-lying states in the spectra of $\Psi^{1/3}_{\mathrm{L-R}}$ matches that with $\Psi^{1/3}_{V_3}$. The counting goes as $1, 2, 5, \ldots$, which is further confirmed (Fig. 5) in the spectra of $N = 10$. This sequence of counting resembles two Abelian edge modes [21]. This indicates that the WYQ 1/3 state has two edge modes rather than one, as evidenced for the Laughlin 1/3 state. Two magnetoroton minima in the neutral mode (Fig. 3) for the bulk excitations is consistent with the two edge modes.

III. CLOSED-FORM WAVE FUNCTION FOR 4/11 STATE

In Ref. [13], the ground-state wave function for $\nu = 4/11$ was proposed as the CF-WYQ wave function,

$$\Psi^{4/11}_{\mathrm{CF-WYQ}} = \mathrm{P}_{\mathrm{LLL}} \prod_{i<j}^{[1,N]} (u_i v_j - u_j v_i)^2\, \Phi^{1+1/3}_{\mathrm{WYQ}}, \tag{8}$$

TABLE III. Overlaps of the wave function $\Psi^{4/11}_{\mathrm{CFD}}$ with $\Psi^{4/11}_{\mathrm{CF-WYQ}}$, $\Psi^{4/11}_{\mathrm{L-R}}$, and $\Psi^{4/11}_{\mathrm{L-MR}}$ for N electrons of which N^* electrons in $\Lambda = 1$ level. The numbers in (..) indicate the Monte Carlo uncertainty in the last significant digits.

N	N^*	$\langle\Psi^{4/11}_{\mathrm{CFD}}\|\Psi^{4/11}_{\mathrm{CF-WYQ}}\rangle$	$\langle\Psi^{4/11}_{\mathrm{CFD}}\|\Psi^{4/11}_{\mathrm{L-R}}\rangle$	$\langle\Psi^{4/11}_{\mathrm{CFD}}\|\Psi^{4/11}_{\mathrm{L-MR}}\rangle$
12	5	1.0	1.0	–
16	6	0.9985(1)	0.893(1)	0.9977(0)
20	7	0.9834(1)	0.976(1)	0.9800(0)
24	8	0.9351(2)	0.892(1)	0.9551(4)
28	9	0.9627(2)	0.790(3)	0.9093(6)

where $\Phi^{1+1/3}_{\mathrm{WYQ}}$ is the determinant with $\Lambda = 0$ completely filled by $N - N^*$ particles and 1/3-filled $\Lambda = 1$ level with $N^* = N/4 + 2$. Here the WYQ wave function for the 1/3 state is the exact numerical wave function (linear combination of $N^* \times N^*$ determinants when N^* particles occupy certain single particle states) for the ground state of the pseudopotential V_3.

As we now have a trial wave function [Eqs. (3) and (4)] for $\Phi^{1/3}_{V_3}$, we explicitly construct the corresponding wave function for $\nu = 4/11$ as

$$\Psi^{4/11}_{L-R} = \prod_{i<j}^{[1,N]} (u_i v_j - u_j v_i)^2\, \mathcal{A}\Bigg[\prod_{k<l}^{[N^*+1,N]} (u_k v_l - u_l v_k) \times \Bigg(\prod_{j}^{[1,N^*]} Q_j\Bigg) \big(D_\alpha \Psi^{1/3,N^*}_{\alpha,\mathrm{L-R}}(\{u_i,\ v_i\})\big)\Bigg], \tag{9}$$

Here antisymmetrization $\mathcal{A}$ may be performed conveniently by multiplying the corresponding factor $(-1)^{\sum_j j}$ with each of the combinations ${}^N C_{N^*}$, where j represents the particle number associated in the second Λ level, the second Λ level projection factor $Q_j = \sum_{l\neq j}^{[1,N]} v_j v_l (u_j v_l - u_l v_j)^{-1}$ into the lowest Λ level, and D_α represents numerical factor (see Appendixes B and C for details) associated with α basis of the DSPEB of $\Psi^{1/3,N^*}_{\mathrm{L-R}}$. However, the detailed numerical factors and need for DSPEB is special for the spherical geometry. The proposed wave function in the disk geometry will have a much simpler structure,

$$\Psi^{4/11}_{\mathrm{L-R}} = \prod_{i<j}^{[1,N]} (z_i - z_j)^2 \mathcal{A}\Bigg[\prod_{k<l}^{[N^*+1,N]} (z_k - z_l) \Bigg(\prod_{j}^{[1,N^*]} P_j\Bigg) \times \Psi^{1/3,N^*}_{\mathrm{L-R}}(\{z_j\})\Bigg] \exp\Bigg[-\frac{1}{4\ell^2}\sum_j |z_j|^2\Bigg], \tag{10}$$

with $P_j = \sum_{l\neq j}^{[1,N]} (z_l - z_j)^{-1}$ and the explicit form of $\Psi^{1/3,N^*}_{\mathrm{L-R}}$ is shown in Eq. (5) for N^* particles.

The overlap of the trial wave function $\Psi^{4/11}_{\mathrm{L-R}}$ (9) with the CFD [24] wave function [13] $\Psi^{4/11}_{\mathrm{CFD}}$ for $\nu = 4/11$ is tabulated in Table III. The overlaps are reasonably high and it is further increased with the trial wave function $\Psi^{4/11}_{\mathrm{L-R}}$ replaced by $\Psi^{4/11}_{\mathrm{L-MR}}$. A comparison has also been made with the overlap $\langle\Psi^{4/11}_{\mathrm{CFD}}|\Psi^{4/11}_{\mathrm{CF-WYQ}}\rangle$ reported earlier [13]. In Fig. 6, we compare the energies corresponding to $\Psi^{4/11}_{\mathrm{CFD}}$, $\Psi^{4/11}_{\mathrm{L-R}}$, and $\Psi^{4/11}_{\mathrm{L-MR}}$

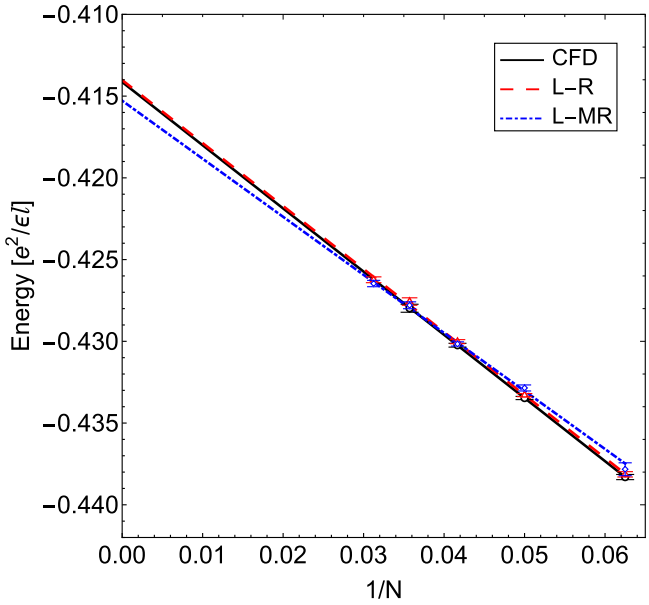

FIG. 6. Ground-state energy per electron versus $1/N$ for $\Psi^{4/11}_{\rm CFD}$ (circles), $\Psi^{4/11}_{\rm L-R}$ (triangles), and $\Psi^{4/11}_{\rm L-MR}$ (diamonds). The corresponding linearly fitted lines are extrapolated to determine the ground-state energies in the thermodynamic limit.

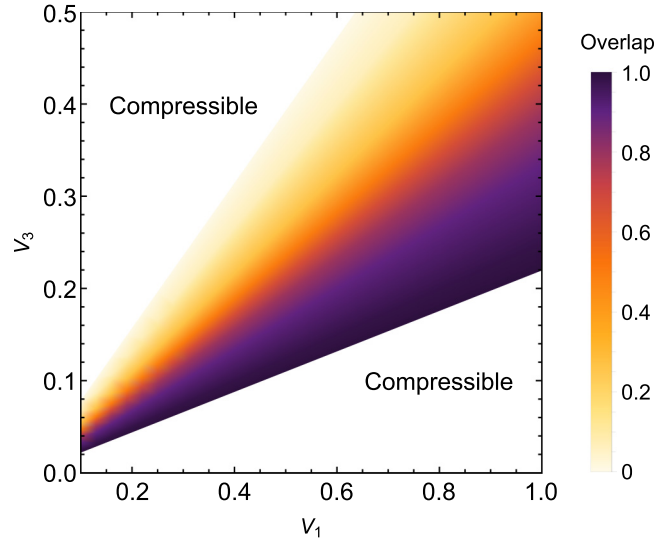

FIG. 7. Phase diagram for $4/11$ state obtained for $N = 12$ electrons. The filled region indicates the regime of incompressible ground state. The gradient in the color coding indicates the overlap of the exact ground state wave function in the hybrid pseudopotentials of V_1 and V_3 with the CFD ground-state wave function. We consider the phase as incompressible when the ground state is obtained at zero angular momentum and no other state is degenerate to this state.

states for various N. The linear extrapolations of these data determine the respective thermodynamic energies per particle as $-0.4141(4)$, $-0.4140(3)$, and $-0.4153(5)$ in the unit $e^2/(\epsilon\ell)$ where ϵ is the dielectric constant of the background. Surprisingly, the energy of the trial wave function is very close to that of the CFD wave function. As the overlaps $\langle\Psi^{4/11}_{\rm CFD}|\Psi^{4/11}_{\rm L-R}\rangle$ for the systems that we have studied are reasonably high and the ground-state energies corresponding to these states in the thermodynamic limit are very close, the trial wave function Eq. (9) may be regarded as a good trial wave function in spherical geometry for the $\nu = 4/11$ state.

IV. PHASE DIAGRAM

We recall that the neighboring conventional states of $4/11$, i.e., $1/3$ and $2/5$ are understood through the model pseudopotential V_1 only. On the other hand, the unconventional incompressible $4/11$ state is understood through a wave function which is partly constructed with a wave function that describes an incompressible state for V_3 pseudopotential. This indicates the $4/11$ state should not be incompressible for V_1 alone, and V_3 pseudopotential must have a substantial role for the state's incompressibility. For investigating whether or not this assertion is true, we obtain a phase diagram (Fig. 7) in V_1–V_3 parameter space by performing exact diagonalization for the $4/11$ state with $N = 12$ electrons and hybrid pseudopotentials and examining the state's nature. Clearly, unlike its neighboring conventional states, the $4/11$ state is not incompressible for V_1 alone. Also, V_3 alone cannot make the $4/11$ state incompressible. A window of $V_3/V_1 < 1$ makes the $4/11$ state incompressible. Because the values of V_1 and V_3 for Coulomb potential in the lowest LL are in the same order of magnitude with $V_1 > V_3$, unconventional states like $4/11$ and $5/13$ are incompressible along with their immediate neighboring conventional states $1/3$ and $2/5$.

V. DISCUSSION

In this paper, we have proposed a trial wave function for the WYQ $1/3$ state in terms of a product of the Laughlin wave function and a ring function in which all electrons are correlated with two other electrons only. The ES of this wave function as well as the exact wave function indicates that this state consists of two edge modes rather than one. This wave function has further been used for the $1/3$-filled second Λ level along with the completely filled lowest Λ level for constructing a wave function for the $4/11$ state. This indicates that the $4/11$ state should have *three* gapless edge modes. It will be interesting to study the currents flowing through each of the channels, thereby determining the charge of the quasiparticle for the $4/11$ state. All our results are based on the calculations on a sphere. We have also proposed analogous trial wave functions for a disk geometry.

Another approach would be development of the conformal field theory for the WYQ $1/3$ state, thereby determining the ground-state wave function followed by proving its adiabatic connection with our proposed wave function.

ACKNOWLEDGMENTS

We thank Ajit Balram for pointing out a mistake in an early version of the paper which was circulated before its first submission for publication. We thank Sutirtha Mukherjee for generously sharing with us the published CFD data. We acknowledge the Param Shakti (IIT Kharagpur)—a National Supercomputing Mission, Government of India for provid-

ing their computational resources. S.S.M. is supported by the Council of Scientific and Industrial Research, Human Resource Development Group, India, through Scheme No. 03(1436)/18/EMR-II.

APPENDIX A: DECOMPOSITION OF A TRIAL MANY-BODY WAVE FUNCTION IN SINGLE-PARTICLE EIGENBASIS

Consider a general many-body wave function with total angular momentum $L = 0$ in a spherical geometry as

$$\Psi = \mathcal{A}\prod_{i<j}^{N}(u_i v_j - u_j v_i)^{n_{ij}}, \tag{A1}$$

where $u_j = \cos(\theta_j/2)e^{i\phi_j/2}$ and $v_j = \sin(\theta_j/2)e^{i\phi_j/2}$ are the spherical spinors for the jth electron in terms of spherical angles $0 \leqslant \theta_j \leqslant \pi$ and $0 \leqslant \phi_j \leqslant 2\pi$, the integer exponent $n_{ij} \geqslant 1$ (requirement due to Pauli exclusion principle) depends on pair of electrons with the constraint $\sum_j n_{ij} = N_\Phi$ for any electron with N_Φ being the total number of flux quanta. In general, n_{ij} may not be equal for all $N(N-1)/2$ pairs and hence antisymmetrization represented by $\mathcal{A}$ must be performed with different permutations of the pairs. We note that the ground-state wave function of any FQHE state can be obtained by diagonalizing the many-body Hamiltonian in the linearly independent many-body basis functions Eq. (A1), which may be obtained for different sets [38] of n_{ij} with the above constraint. Considering $\eta_j = u_j/v_j$, the wave function in Eq. (A1) can be recast as

$$\Psi = \prod_j v_j^{N_\Phi}\Phi(\{\eta_j\})\ ;\ \Phi(\{\eta_j\}) = \mathcal{A}\prod_{i<j}^{N}(\eta_i - \eta_j)^{n_{ij}}\ , \tag{A2}$$

where $\Phi(\{\eta_j\})$ is an antisymmetric polynomial of degree $NN_\Phi/2$. We then factor out the Vandermonde determinant $V = \prod_{i<j}^{N}(\eta_i - \eta_j)$ from the function $\Phi(\{\eta_j\})$, i.e.,

$$\Phi(\{\eta_j\}) = V\tilde{\Phi}(\{\eta_j\})\ ;\ \tilde{\Phi}(\{\eta_j\}) = \mathcal{S}\prod_{i<j}^{N}(\eta_i - \eta_j)^{n_{ij}-1} \tag{A3}$$

will be a symmetric polynomial of degree $N(N_\Phi - N + 1)/2$, where $\mathcal{S}$ represents the symmetrization over the permutation of particles.

The symmetric polynomial $\tilde{\Phi}(\{\eta_j\})$ can be expressed in the symmetric monomial [39] basis $M_{\{\mu\}}$ given by

$$M_{\{\mu\}} = \sum_{P_{\{\mu\}}}\prod_{i=1}^{N}\eta_i^{\{\mu\}}, \tag{A4}$$

with distinct set $\{\mu\} \equiv (\mu_1, \mu_2, \ldots, \mu_{_N})$ in descending order such that $0 \leqslant \mu_i \leqslant N_\Phi - N + 1$ and $\sum_{i=1}^{N}\mu_i = N(N_\Phi - N + 1)/2$. Here the summation over $P_{\{\mu\}}$ represents all the permutations of the entries in the set $\{\mu\}$. We thus have [40]

$$\tilde{\Phi}(\{\eta_j\}) = \sum_\alpha m_\alpha M_{\alpha\equiv\{\mu\}}, \tag{A5}$$

where we associate a number α for a distinct set of $\{\mu\}$, the dimension of α is equal to the number of distinct symmetric polynomials, and the coefficient m_α is the weight factor of the symmetric polynomial M_α.

The symmetrization in Eq. (A3) involves addition of $N!$ terms of the permutation, in general. It is a rather daunting task even with the use of MATHEMATICA [41] for algebraic manipulation with such a huge number of terms because each term consists of several monomial basis functions. We, however, exploit the form of the function $\prod_{i<j}^{N}(\eta_i - \eta_j)^{n_{ij}-1}$ for one of the terms of the permutation to obtain m_α without explicit consideration of other $(N! - 1)$ terms. We first expand $\prod_{i<j}^{N}(\eta_i - \eta_j)^{n_{ij}-1}$ as a sum of terms, each as products of the monomials in all the coordinates η_i. These terms belong to several groups identified with the appropriate set α. By adding the coefficients of all the terms in a set α, we find m'_α. We then inspect entries of μ_i in the set $\alpha \equiv (\mu_1, \mu_2, \ldots, \mu_{_N})$ and count the number of equal entries. If all the μ_i's are different, m'_α gets renormalized for all the $N!$ terms. However, if there are n_λ identical entries with $\lambda = 1, \ldots, k$, then m'_α normalizes to

$$m_\alpha = m'_\alpha\prod_{\lambda=1}^{k} n_\lambda!\,. \tag{A6}$$

The symmetric polynomial $\tilde{\Phi}(\{\eta_j\})$ can also be expanded in the Schur basis [39], where the Schur functions are given by

$$S_{\{\mu\}}(\eta_1, \eta_2, \ldots, \eta_N) \equiv \frac{\begin{vmatrix} \eta_1^{\mu_1+N-1} & \eta_1^{\mu_2+N-2} & \cdots & \eta_1^{\mu_N} \\ \eta_2^{\mu_1+N-1} & \eta_2^{\mu_2+N-2} & \cdots & \eta_2^{\mu_N} \\ \vdots & \vdots & \ddots & \vdots \\ \eta_N^{\mu_1+N-1} & \eta_N^{\mu_2+N-2} & \cdots & \eta_N^{\mu_N} \end{vmatrix}}{\begin{vmatrix} \eta_1^{N-1} & \eta_1^{N-2} & \cdots & 1 \\ \eta_2^{N-1} & \eta_2^{N-2} & \cdots & 1 \\ \vdots & \vdots & \ddots & \vdots \\ \eta_N^{N-1} & \eta_N^{N-2} & \cdots & 1 \end{vmatrix}}. \tag{A7}$$

We thus have [40]

$$\tilde{\Phi}(\{\eta_j\}) = \sum_\alpha s_\alpha S_{\alpha\equiv\{\mu\}}(\{\eta_j\})\,, \tag{A8}$$

where the Schur coefficients s_α are to be determined.

From combinatorial theory, the Schur basis functions Eq. (A7) is identified as a sum of monomials over semistandard Young tableaux (SSYT) of shape $\alpha \equiv (\mu_1, \mu_2, \ldots, \mu_{_N})$ and which are in turn related to monomial symmetric basis functions Eq. (A4):

$$S_\alpha(\eta_1, \eta_2, \ldots, \eta_{_N}) = \sum_\beta K_{\alpha\beta}M_\beta(\eta_1, \eta_2, \ldots, \eta_{_N})\,. \tag{A9}$$

The non-negative integer element $K_{\alpha\beta}$ is the number of SSYT of shape α and weight β, called a Kostka number [39]. The matrix K which we evaluate here using SAGEMATH [42] is an upper-triangular matrix with unity diagonal elements. Using Eqs. (A5), (A8), and (A9), we find

$$m_\beta = \sum_\alpha s_\alpha K_{\alpha\beta}, \tag{A10}$$

which determines s_α as

$$s_\alpha = m_\alpha - \sum_{\beta=1}^{\alpha-1} s_\beta K_{\beta\alpha}\,. \tag{A11}$$

In the spherical geometry, the single-particle eigenfunctions for the lowest LL are given by [5]

$$\phi_\lambda(u,v) = \left[\frac{2Q+1}{4\pi}\binom{2Q}{Q-\lambda}\right]^{1/2}(-1)^{Q-\lambda}v^{Q-\lambda}u^{Q+\lambda}, \tag{A12}$$

where $2Q = N_\Phi$ is the total number of flux quanta, $\lambda = -Q, -Q+1, \ldots, +Q$ indicate quantum numbers of the degenerate states in the lowest LL. By defining $Q+\lambda = l$ and $\eta = u/v$, we find

$$\phi_l(u,v) = v^{2Q}\mathcal{N}_l\eta^l\ ;\ \mathcal{N}_l = \left[\frac{2Q+1}{4\pi}\binom{2Q}{l}\right]^{1/2}(-1)^l, \tag{A13}$$

with $l = 0, 1, \ldots, 2Q$. Therefore, the Schur functions Eq. (A7) can be constructed with the single-particle basis functions Eq. (A13). The determinant in the numerator of the Schur functions are then related with the many electron basis functions which can be expressed in terms of single particle basis functions.

Equations (A2), (A3), (A7), (A8), and (A13) determine Ψ with many-body determinant basis functions as

$$\Psi = \sum_\alpha \frac{s_\alpha}{\prod_{i=1}^N \mathcal{N}_{\mu_i+N-i}} \times \begin{vmatrix} \phi_{\mu_1+N-1}(1) & \phi_{\mu_2+N-2}(1) & \cdots & \phi_{\mu_N}(1) \\ \phi_{\mu_1+N-1}(2) & \phi_{\mu_2+N-2}(2) & \cdots & \phi_{\mu_N}(2) \\ \vdots & \vdots & \ddots & \vdots \\ \phi_{\mu_1+N-1}(N) & \phi_{\mu_2+N-2}(N) & \cdots & \phi_{\mu_N}(N) \end{vmatrix}, \tag{A14}$$

where $l = 0, \ldots, 2Q$ in $\phi_l(i)$ are the spherical quantum numbers, (i) is the shorthand of (u_i, v_i), and $\alpha \equiv (\mu_1, \ldots, \mu_N)$.

Example: As an illustration for the use of the above algorithm, we consider the Moore-Read wave function [15] in spherical geometry for $N = 4$ with $N_\Phi = 2Q = 5$:

$$\Psi_{\rm MR} = \sum_{i<j}^{4}(u_iv_j - u_jv_i)^2\,{\rm Pf}\left(\frac{1}{u_iv_j - u_jv_i}\right), \tag{A15}$$

$$= \prod_{j=1}^{4} v_j^5 \prod_{i<j}^{4}\eta_{ij}^2\mathcal{A}\left(\frac{1}{\eta_{13}\eta_{24}}\right), \tag{A16}$$

where $\eta_{ij} = \eta_i - \eta_j$ and ${\rm Pf}(A)$ represents Pfaffian of the antisymmetric matrix A. We thus find

$$\tilde{\Phi}(\{\eta_j\}) = \mathcal{S}[\eta_{12}\eta_{14}\eta_{23}\eta_{34}]\,. \tag{A17}$$

As prescribed above, without performing explicit symmetrization here, we just consider the bracketed term above, i.e., the polynomial $P(\{\eta_j\}) = \eta_{12}\eta_{14}\eta_{23}\eta_{34}$. An expansion of $P(\{\eta_j\})$ yields

$$\begin{aligned} P(\{\eta_j\}) = &\left(-\eta_1^2\eta_3^2 - \eta_2^2\eta_4^2\right) + \left(\eta_1^2\eta_2\eta_3 - \eta_1^2\eta_2\eta_4\right. \\ &+\eta_1^2\eta_3\eta_4 + \eta_4^2\eta_1\eta_2 + \eta_4^2\eta_2\eta_3 - \eta_4^2\eta_1\eta_3 \\ &-\eta_2^2\eta_1\eta_3 + \eta_2^2\eta_1\eta_4 + \eta_2^2\eta_3\eta_4 + \eta_3^2\eta_1\eta_4 \\ &\left.+\eta_3^2\eta_1\eta_2 - \eta_3^2\eta_2\eta_4\right) + (-2\eta_1\eta_2z\eta_3\eta_4), \end{aligned} \tag{A18}$$

which corresponds to three sets of $\{\mu\}$, namely, (2,2,0,0), (2,1,1,0), and (1,1,1,1) denoted by $\alpha = 1$, 2, and 3, respectively. Therefore, $\tilde{\Phi}(\{\eta_j\})$ is the addition of M_1, M_2, and M_3 which, respectively, are the symmetric monomials constructed upon symmetrization of the respective group of terms within the parentheses in Eq. (A18). We find $m_1' = -2$, $m_2' = 4$, and $m_3' = -2$, which are the sum of the coefficients of these respective groups. In the sets, two entries occur twice, one entry occurs twice and two entries occur once, and one entry occurs four times, respectively, for $\alpha = 1$, 2, and 3. Therefore, $m_1 = m_1' \times 2!2! = -8$, $m_2 = m_2' \times 2!1!1! = 8$, and $m_3 = m_3' \times 4! = -48$.

We now determine the upper triangular K matrix whose nonzero elements $K_{\alpha\beta}$ are the Kostka numbers [39] describing the number of SSYT possible of shape α and weight β, where α and β describe three sets, namely, (2,2,0,0), (2,1,1,0), and (1,1,1,1). We thus find

$$K = \begin{pmatrix} 1 & 1 & 2 \\ 0 & 1 & 3 \\ 0 & 0 & 1 \end{pmatrix}. \tag{A19}$$

We next evaluate s_α using Eqs. (A11) and (A19) and find $s_1 = -8$, $s_2 = 16$, and $s_3 = -80$. Using Eq. (A14), we therefore find (ignoring overall constant factor)

$$\begin{aligned} \Psi_{\rm MR} \equiv &\frac{1}{\sqrt{3}}\begin{vmatrix} \phi_5(1) & \phi_4(1) & \phi_1(1) & \phi_0(1) \\ \phi_5(2) & \phi_4(2) & \phi_1(2) & \phi_0(2) \\ \phi_5(3) & \phi_4(3) & \phi_1(3) & \phi_0(3) \\ \phi_5(4) & \phi_4(4) & \phi_1(4) & \phi_0(4) \end{vmatrix} \\ &-\frac{1}{\sqrt{3}}\begin{vmatrix} \phi_5(1) & \phi_3(1) & \phi_2(1) & \phi_0(1) \\ \phi_5(2) & \phi_3(2) & \phi_2(2) & \phi_0(2) \\ \phi_5(3) & \phi_3(3) & \phi_2(3) & \phi_0(3) \\ \phi_5(4) & \phi_3(4) & \phi_2(4) & \phi_0(4) \end{vmatrix} \\ &+\frac{1}{\sqrt{3}}\begin{vmatrix} \phi_4(1) & \phi_3(1) & \phi_2(1) & \phi_1(1) \\ \phi_4(2) & \phi_3(2) & \phi_2(2) & \phi_1(2) \\ \phi_4(3) & \phi_3(3) & \phi_2(3) & \phi_1(3) \\ \phi_4(4) & \phi_3(4) & \phi_2(4) & \phi_1(4) \end{vmatrix}, \end{aligned} \tag{A20}$$

which is precisely the same as the exact ground-state description of three-body pseudo-potential for which the Moore-Read [15] wave function is exact.

APPENDIX B: SINGLE-PARTICLE BASIS FUNCTIONS FOR FIRST AND SECOND Λ LEVELS IN SPHERICAL GEOMETRY

For the ^{2}CFs, the effective monopole flux $2q = 2Q - 2(N-1)$ and thus quantum numbers $m = -q, -q+1, \ldots, q$ and $m = -(q+1), -q, \ldots, (q+1)$ are present for single-particle basis functions, respectively, in $\Lambda = 0$ and 1.

The eigenbasis function in $\Lambda = 0$ are given by

$$\tilde{\phi}_m^{(0)}(u,v) = \left[\frac{2q+1}{4\pi}\binom{2q}{q-m}\right]^{1/2}(-1)^{q-m}v^{q-m}u^{q+m}, \tag{B1}$$

which may be written for the jth particle as

$$\tilde{\phi}_l^{(0)}(j) \sim (-1)^l \left(\frac{1}{l!(2q-l)!}\right)^{1/2} v_j^{2q}\, \eta_j^l \tag{B2}$$

(up to the l-dependent part of normalization factor) with $l = 0, 1, \ldots, 2q$ and $\eta_j = u_j/v_j$, by defining $l = q + m$.

The single-particle eigenfunctions in $\Lambda = 1$ are given by

$$\begin{aligned}\tilde{\phi}_m^{(1)}(u, v) = &\left[\frac{2q+3}{4\pi}\frac{(q+1-m)!(q+1+m)!}{(2q+1)!}\right]^{1/2} \\ &\times \left[\binom{2q+1}{q+1-m} vv^* - \binom{2q+1}{q+1+m} uu^*\right] \\ &\times (-1)^{q+1-m} v^{q-m} u^{q+m},\end{aligned} \tag{B3}$$

with $m = -(q+1), -q, \ldots, (q+1)$; while the first term in the bracket is excluded for $m = -(q+1)$, the second term is excluded for $m = q+1$. The lowest-LL projected basis functions are then found to be for the jth particle [25] as

$$\begin{aligned}\tilde{\phi}_{l,\mathrm{proj}}^{(1)} = \mathcal{N}_l^{(1)} v_j^{2q} \eta_j^l \Bigg[&\binom{2q+1}{l-1}\left(Q_j - \frac{N-1}{\eta_j}\right) \\ &+ \binom{2q+1}{l} Q_j\Bigg],\end{aligned} \tag{B4}$$

with $l = q+1+m$, i.e., $l = 0, 1, \ldots, 2(q+1)$, ($l \neq 0$ for the first term and $l \neq 2(q+1)$ in the second term inside the bracket), $\eta_j = u_j/v_j$, $Q_j = \sum_{k\neq j}(v_j v_k)/(u_j v_k - u_k v_j)$, and $\mathcal{N}_l^{(1)} = [\frac{2q+3}{4\pi}\frac{(2q+2-l)!l!}{(2q+1)!}]^{1/2}(-1)^l$. Now dropping the functions which are already included in the basis functions of $\Lambda = 0$, we find the basis states (keeping only the l-dependent constant factor of the normalization constant),

$$\begin{aligned}\tilde{\phi}_{l,\mathrm{proj}}^{(1)}(j) \sim (-1)^l &\left(\frac{1}{l!(2q+2-l)!}\right)^{1/2} v_j^{2q}\eta_j^l \\ &\times \begin{cases} l\left(Q_j - \frac{N-1}{\eta_j}\right) & \text{for } l = 2(q+1) \\ Q_j & \text{otherwise.}\end{cases}\end{aligned} \tag{B5}$$

We note that Eqs. (B2) and (B5) have close resemblance with the corresponding wave functions in disk geometry [5].

APPENDIX C: CONVERSION OF MANY-BODY WAVE FUNCTION FOR LOWEST LANDAU LEVEL TO $\Lambda = 1$ LEVEL

Using the method of DSPEB developed above, we can decompose $\Psi_{\mathrm{L-R}}^{1/3,N^*}$ for N^* particles in terms of single-particle basis $\tilde{\phi}_l^{(0)}$ [see Eq. (B2)] of $\Lambda = 0$ as

$$\begin{aligned}\Psi_{\mathrm{L-R}}^{1/3,N^*}\big|_{\Lambda=0} &= \sum_\alpha C_\alpha \begin{vmatrix} \tilde{\phi}_{l_1}^{(0)}(1) & \tilde{\phi}_{l_2}^{(0)}(1) & \cdots & \tilde{\phi}_{l_{N^*}}^{(0)}(1) \\ \tilde{\phi}_{l_1}^{(0)}(2) & \tilde{\phi}_{l_2}^{(0)}(2) & \cdots & \tilde{\phi}_{l_{N^*}}^{(0)}(2) \\ \vdots & \vdots & \vdots & \vdots \\ \tilde{\phi}_{l_1}^{(0)}(N^*) & \tilde{\phi}_{l_2}^{(0)}(N^*) & \cdots & \tilde{\phi}_{l_{N^*}}^{(0)}(N^*) \end{vmatrix}_\alpha .\end{aligned} \tag{C1}$$

For constructing $\Psi_{\mathrm{L-R}}^{1/3,N^*}$-like wave functions in $\Lambda = 1$, we need to replace $\tilde{\phi}_{l_i}^{(0)}$ by $\tilde{\phi}_{l_i}^{(1)}$ in Eq. (C1). Now exploiting the common terms in the expression of $\tilde{\phi}_{l_i}^{(0)}$ and $\tilde{\phi}_{l_i}^{(1)}$ [see Eqs. (B2) and (B5)], we are able to express

$$\begin{aligned}\Psi_{\mathrm{L-R}}^{1/3,N^*}\big|_{\Lambda=1} = &\prod_{j=1}^{N^*} Q_j \sum_\alpha D_\alpha \\ &\times \begin{vmatrix} \tilde{\phi}_{l_1}^{(0)}(1) & \tilde{\phi}_{l_2}^{(0)}(1) & \cdots & \tilde{\phi}_{l_{N^*}}^{(0)}(1) \\ \tilde{\phi}_{l_1}^{(0)}(2) & \tilde{\phi}_{l_2}^{(0)}(2) & \cdots & \tilde{\phi}_{l_{N^*}}^{(0)}(2) \\ \vdots & \vdots & \vdots & \vdots \\ \tilde{\phi}_{l_1}^{(0)}(N^*) & \tilde{\phi}_{l_2}^{(0)}(N^*) & \cdots & \tilde{\phi}_{l_{N^*}}^{(0)}(N^*) \end{vmatrix}_\alpha ,\end{aligned} \tag{C2}$$

with an exception that $\tilde{\phi}_{2q+2}^{(0)}(j)$ should be multiplied by the factor $1 - (N-1)/(\eta_j Q_j)$

$$D_\alpha = C_\alpha \prod_{i=1}^{N^*} \left(\frac{1}{(2q+2-l_i)(2q+1-l_i)}\right)^{1/2} . \tag{C3}$$

[1] D. C. Tsui, H. L. Stormer, and A. C. Gossard, Phys. Rev. Lett. **48**, 1559 (1982).
[2] R. B. Laughlin, Phys. Rev. Lett. **50**, 1395 (1983).
[3] K. V. Klitzing, G. Dorda, and M. Pepper, Phys. Rev. Lett. **45**, 494 (1980).
[4] J. K. Jain, Phys. Rev. Lett. **63**, 199 (1989); Phys. Rev. B **41**, 7653 (1990).
[5] J. K. Jain, *Composite Fermions* (Cambridge University Press, New York, 2007).
[6] G. A. Csáthy in *Frational Quantum Hall Effects: New Developments*, edited by B. I. Halperin and J. K. Jain (World Scientific, New Jersey, 2020).
[7] W. Pan, H. L. Stormer, D. C. Tsui, L. N. Pfeiffer, K. W. Baldwin, and K. W. West, Phys. Rev. Lett. **90**, 016801 (2003).
[8] W. Pan, K. W. Baldwin, K. W. West, L. N. Pfeiffer, and D. C. Tsui, Phys. Rev. B **91**, 041301(R) (2015).
[9] N. Samkharadze, I. Arnold, L. N. Pfeiffer, K. W. West, and G. A. Csáthy, Phys. Rev. B **91**, 081109(R) (2015).
[10] S. Mukherjee and S. S. Mandal, Phys. Rev. Lett. **114**, 156802 (2015).
[11] A. C. Balram, Phys. Rev. B **94**, 165303 (2016).
[12] S. Mukherjee, S. S. Mandal, A. Wójs, and J. K. Jain, Phys. Rev. Lett. **109**, 256801 (2012).
[13] S. Mukherjee, S. S. Mandal, Y.-H. Wu, A. Wójs, and J. K. Jain, Phys. Rev. Lett. **112**, 016801 (2014).
[14] S. Mukherjee, J. K. Jain, and S. S. Mandal, Phys. Rev. B **90**, 121305(R) (2014).
[15] G. Moore and N. Read, Nucl. Phys. B **360**, 362 (1991).
[16] A. Wójs, K.-S. Yi, and J. J. Quinn, Phys. Rev. B **69**, 205322 (2004).
[17] F. D. M. Haldane, Phys. Rev. Lett. **51**, 605 (1983).
[18] S. M. Girvin, Phys. Rev. B **30**, 558 (1984).

[19] S. M. Girvin, A. H. MacDonald, and P. M. Platzman, Phys. Rev. B **33**, 2481 (1986).
[20] H. Li and F. D. M. Haldane, Phys. Rev. Lett. **101**, 010504 (2008).
[21] X. G. Wen, Adv. Phys. **44**, 405 (1995).
[22] P. Sitko, S. N. Yi, K. S. Yi, and J. J. Quinn, Phys. Rev. Lett. **76**, 3396 (1996).
[23] S.-Y. Lee, V. W. Scarola, and J. K. Jain, Phys. Rev. Lett. **87**, 256803 (2001).
[24] S. S. Mandal and J. K. Jain, Phys. Rev. B **66**, 155302 (2002).
[25] S. S. Mandal, J. Phys. Condens. Matter **30**, 405605 (2018).
[26] Diagham: http://nick-ux.lpa.ens.fr/diagham/wiki.
[27] R. K. Kamilla, J. K. Jain, and S. M. Girvin, Phys. Rev. B **56**, 12411 (1997).
[28] S. M. Girvin, A. H. MacDonald, and P. M. Platzman, Phys. Rev. Lett. **54**, 581 (1985).
[29] N. Read and E. Rezayi, Phys. Rev. B **54**, 16864 (1996).
[30] R. H. Morf, N. d'Ambrumenil, and S. Das Sarma, Phys. Rev. B **66**, 075408 (2002).
[31] A. Chandran, M. Hermanns, N. Regnault, and B. A. Bernevig, Phys. Rev. B **84**, 205136 (2011).
[32] I. D. Rodríguez, S. C. Davenport, S. H. Simon, and J. K. Slingerland, Phys. Rev. B **88**, 155307 (2013).
[33] I. D. Rodríguez, S. H. Simon, and J. K. Slingerland, Phys. Rev. Lett. **108**, 256806 (2012).
[34] J. Dubail, N. Read, and E. H. Rezayi, Phys. Rev. B **85**, 115321 (2012).
[35] A. Sterdyniak, A. Chandran, N. Regnault, B. A. Bernevig, and P. Bonderson, Phys. Rev. B **85**, 125308 (2012).
[36] R. Thomale, A. Sterdyniak, N. Regnault, and B. A. Bernevig, Phys. Rev. Lett. **104**, 180502 (2010).
[37] M. A. Nielsen and I. L. Chuang, *Quantum Computation and Quantum Information* (Cambridge University Press, Cambridge, 2000).
[38] S. Das, S. Das, and S. S. Mandal (unpublished).
[39] I. G. Macdonald, *Symmetric Functions and Hall Polynomials* (Oxford Science Publication, New York, 1979).
[40] S. S. Mandal, S. Mukherjee, and K. Ray, Ann. Phys. **390**, 236 (2018).
[41] Wolfram Research, Inc., Mathematica, Version 12.1, Champaign, IL (2020).
[42] SageMath, the Sage Mathematics Software System, Version 8.7, The Sage Developers, 2019, https://www.sagemath.org.